A Random Forest-Assisted Fast Distributed Auction-Based Algorithm for Hierarchical Coordinated Power Control in a Large-Scale PV Power Plant

Xiaoshun Zhang, *Member*, *IEEE*, Tao Yu, *Member*, *IEEE,* Bo Yang, and Lin Jiang, *Member, IEEE*

Abstract—In response to the automatic generation control (AGC) signals, the direct power control of a large-scale PV power plant easily encounters the communication bottlenecks, the high optimization difficulty and computation burden due to the large number of controllable inverters with different response performances. To handle these problems, a hierarchical framework of coordinated power control (CPC) is constructed, which is decomposed into a upper-layer CPC between different sub-areas and a lower-layer CPC between different inverters in each sub-area. Instead of a centralized optimization, a novel random forest-assisted fast distributed auction-based algorithm (FDAA) is proposed for a distributed optimization of CPC. The random forest can rapidly generate a dynamic surrogate model of the optimization results from the low-layer CPC to the upper-layer CPC, thus these two-layer optimizations of CPC can be decoupled without too much interactions and computations. The effectiveness of the proposed method is thoroughly evaluated on a PV power plant with 10 sub-areas and 100 inverters under various irradiation conditions.

Index Terms—PV power plant, hierarchical coordinated power control, fast distributed auction-based algorithm, random forest, surrogate model.

I. Introduction

In recent decade, many new reserve sources, e.g., wind farms and electric vehicles, have participated in automatic generation control (AGC) [1] due to their faster response speed and higher ramp rate compared with the traditional thermal and hydro power plants. Among them, the PV power can be regarded as one of the most promising reserve source [2] owing to its inexhaustibility, near-zero emission and pollution, zero noise, and less maintenance.

Along with these advantages, extensive studies on AGC with the PV power participation have been carried out. To acquire a superior control performance of the control area, a neurofuzzy controller [3] and a multi-stage fuzzy assisted PID with filter-(1+PI) [4] have been design for frequency control with PV system, respectively. On the other hand, various control methods were designed to improve the frequency control performance of the grid-connected inverter, including the model predictive control method [5], the curtailment power-current curve based tracking control algorithm [6], a coordination strategy for virtual inertia control and frequency damping control [7], and so on. To achieve a coordinated control between the PV power plant and other reserve resources, a lifelong learning [8] was designed for AGC dispatch with various units. In [9], the conventional AGC dispatch of power system was extended the integrated energy system, in which PV power plant and other energy resources can be effectively coordinated via the deep reinforcement learning. All of these studies mainly focused on the controller and the coordinated strategy for various reserve resources, which did not investigate the coordinated power control between multiple inverters in a large-scale PV power plant.

So far, a frequently-used coordinated control method for multiple inverters is the proportional power allocation of their regulation capacities [10], in which the regulation capacity can be evaluated according to the current operation point and the maximum power point. Besides, the on-off switching control method is usually designed to enable the PV power plant for frequency control [11], especially for a large-scale PV power plant with numerous string inverters [12]. However, these works did not consider the dynamic response performance difference among multiple inverters, while the influence on the reactive power reserve was ignored. As a result, it easily leads to a poor dynamic response performance and an inadequate reactive power reserve for the whole PV power plant in response to the AGC signals. To fill this gap, this paper proposes a new coordinated power control (CPC) for multiple inverters to take both of the dynamic response performance difference and the reactive power reserve into account.

Under the direct control framework [13], the control center should communicate with all the inverters and figure out the optimal solution of CPC. It easily results in a communication bottlenecks, a high optimization difficulty and a computation burden due to the large number of controllable inverters. In contrast, a hierarchical control framework [12] can naturally eliminate these issues via the multi-layer decomposition of CPC. In essence, the CPC of each layer is a nonlinear optimization, which can be solved with the centralized and distributed control manners. In general, the centralized control manner [14] not only needs a high-bandwidth communication infrastructure, but also easily leads to the modeling error and the low reliability under a single point-of-failure. Compared with that, the distributed control manner [15] with the high reliability is easy to be scalable and satisfy the plug-and-play requirement, while the local controllers only require sparse communication infrastructures to exchange limited information. Therefore, a hierarchical framework with the distributed control manner is employed for CPC in this work.

General speaking, the distributed optimization algorithm can be divided into the gradient-based and gradient-free algorithms. The application flexibility of the gradient-based algorithms is low since they are highly dependent on the optimization's

mathematical model. For example, the consensus algorithm [16],[17] is only available for economic dispatch with a common optimal incremental cost corresponding to the minimum point. The alternating direction multiplier method (ADMM) [18] can be implemented for a fully distributed optimization only when the aggregated information is replaced by the distributed acquirement information via an improved calculation without a control center. On the contrary, the gradient-free algorithms are more flexible to implement a distributed optimization owing to the model-free feature. Nevertheless, many meta-heuristic based gradient-free algorithms, e.g., the distributed particle swarm optimization [19] they easily consume a long computation time and lead to a random optimum as a consequence of the random searching operator. Consequently, they are difficult to satisfy the real-time optimization of CPC with the several seconds of control requirement, while the optimum quality can not be guaranteed. In [20], a deterministic and fully distributed auction-based algorithm (AA) was proposed for nonconvex economic dispatch. Compared with AA, an adaptive distributed AA (ADAA) [21] employed an adaptive swap size instead of multiple fixed swap sizes, which not only can reduce the communication complexity, but also can shorten the computation time with a faster convergence rate. It is also suitable to handle the CPC of each layer due to its fast and stable convergence.

Under the hierarchical framework, the upper-layer CPC and lower-layer CPC should be collaborated to find a high-quality optimal control solution. This will cause an expensive computation since the current solution of each agent in the upper-layer CPC can be evaluate only based on the optimization results from the lower-layer CPC. To avoid the high computation cost, the surrogate model [22] has become a popular and powerful technique to accelerate the computation rate of the optimization algorithms. Based on the same way for ADAA, this paper proposes a novel random forest-assisted fast distributed AA (FDAA) for CPC of a large-scale PV power plant, which contains the following novelties:

- The presented CPC firstly considers both of the dynamic response performance difference and the reactive power reserve when a PV power plant is responding to the AGC signals. Hence, multiple inverters can be effectively coordinated to improve the dynamic response performance and the reactive power reserve of the whole PV power plant.
- Under the hierarchical framework, the FDAA based CPC can effectively achieve a fully distributed optimization with a sparse communication, thus the communication bottlenecks, the high optimization difficulty, and the computation burden can be directly avoided.
- Compared with ADAA, the main improvement of FDAA is that it can implement a rapid bid evaluation for computationally expensive optimization problems by introducing a random forest [23] based dynamic surrogate model instead of the original objective function. For the hierarchical CPC, FDAA can directly decouple the low-layer CPC and the upper-layer CPC with the dynamic surrogate model, thus the real-time optimization requirement can be satisfied with much less computation cost and communications.

The remaining sections are organized as follows: Section II gives the framework and mathematical model of CPC. Section III gives the optimization principle of FDAA and the detailed design for CPC. The simulation results and discussions are provided in Section IV. Finally, Section V concludes the paper.

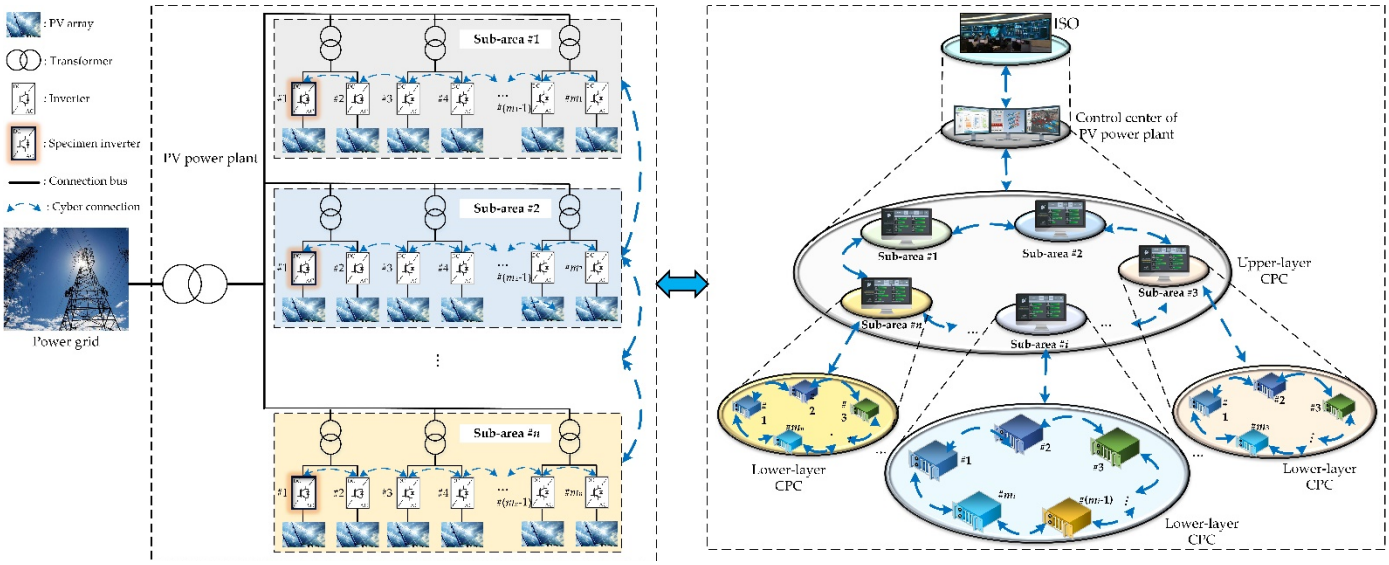

Fig. 1. Hierarchical and distributed control framework of CPC in a large-scale PV power plant.

II. Framework and Mathematical Model of CPC

A. Control Framework

The large-scale PV power plant can be divided into multiple sub-areas in the physical plane, as shown in Fig. 1. Each sub-area consists of multiple PV arrays and inverters, which one of the inverters is taken as the specimen inverter [12] to acquire the real-time maximum power capacity. Furthermore, each inverter is connected with a PV array, while two adjacent inverters are connect with a transformer [24]. Note that each specimen inverter does not participate in AGC, which is operated at the maximum power point under various weather conditions.

In this work, the hierarchical CPC of a PV power plant is essentially an AGC dispatch problem. Particularly, it should distribute the AGC signal of the whole PV power plant to all the controllable inverters. Therefore, the proposed control framework of CPC mainly contains three processes, as follows:

- Firstly, the PV power plant will evaluate its real-time regulation capacity and then transmit it to the independent system operator (ISO). By contrast, ISO will assign real-time AGC signals to the PV power plant.
- Secondly, the local control center of each sub-area will implement a distributed optimization of upper-layer CPC based on the total generation command from the control center of PV power plant.
- Finally, the controller of each inverter will implement a distributed optimization of lower-layer CPC based on the total generation command of the corresponding sub-area.

B. Dynamic Response Model of Inverters

The proposed CPC is mainly used for distributing the AGC signal of the whole PV power plant to all the controllable inverters. Then each inverter will execute the power trace control according to the reference active power input. Hence, CPC cannot acquire the practical regulation power output of each inverter in advance. To quantitatively evaluate the dynamic power regulation performance of each inverter, an equivalent model is adopted approximate the actual regulation power outputs with different input signals. Compared with a detailed and complex dynamic model for an inverter [25], the presented equivalent model can acquire a competitive model accuracy with less information inputs due to the less approximating modules. It consists of three parts [21], including the time delay, the power regulation, and the power limiter, as shown in Fig. 2. The time delay is mainly resulted from the signals communication, while power regulation represents the control process of the inverter controller. By considering these two parts, the presented model can a rapid calculation for the regulation power output of the inverter based on an inverse Laplace transformation [26], as

$$\Delta P_{iw}^{\mathrm{out}}(t) = L^{-1}\left[\frac{e^{-sT_{iw}^{\mathrm{d}}}}{s\left(1+sT_{iw}^{\mathrm{r}}\right)} \cdot \sum_{k=1}^{K}\left[e^{-\Delta T\cdot(k-1)s} \cdot \Delta P_{iw}^{\mathrm{in}}(k)\right]\right] \quad (1)$$

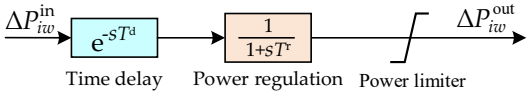

Fig. 2. Equivalent dynamic response model of an inverter.

$$\Delta P_{iw}^{\mathrm{in}}(k) = P_{iw}^{\mathrm{in}}(k) - P_{iw}^{\mathrm{in}}(k-1) \quad (2)$$

$$\Delta P_{iw}^{\mathrm{out}}(k) = \Delta P_{iw}^{\mathrm{out}}(t = \Delta T \cdot k) \quad (3)$$

where $\Delta P_{iw}^{\mathrm{in}}$ and $\Delta P_{iw}^{\mathrm{out}}$ are the regulation power input and output of the *w*th inverter in the *i*th sub-area, respectively; T_{iw}^{d} and T_{iw}^{r} are the delay and regulation time constants, respectively; *k* is the *k*th control interval; $P_{iw}^{\mathrm{in}}(k)$ is the AGC signal of the *w*th inverter in the *i*th sub-area; ΔT is the control cycle; and *K* is the number of the control intervals up to now.

Besides, the real-time regulation capacity of each inverter can be determined by its last AGC signal and the current operation point of the specimen inverter, as follows:

$$\Delta P_{iw}^{\min}(k) \le \Delta P_{iw}^{\mathrm{in}}(k) \le \Delta P_{iw}^{\max}(k) \quad (4)$$

$$\Delta P_{iw}^{\min}(k) = \begin{cases} 0, & \text{if } \Delta P^{\mathrm{in}}(k) \ge 0 \\ P_{iw}^{\min} - P_{iw}^{\mathrm{in}}(k-1), & \text{else} \end{cases} \quad (5)$$

$$\Delta P_{iw}^{\max}(k) = \begin{cases} P_i^{\mathrm{si}}(k) - P_{iw}^{\mathrm{in}}(k-1), & \text{if } \Delta P^{\mathrm{in}}(k) \ge 0 \\ 0, & \text{else} \end{cases} \quad (6)$$

$$\Delta P^{\mathrm{in}}(k) = P^{\mathrm{in}}(k) - P^{\mathrm{in}}(k-1) \quad (7)$$

where $\Delta P_{iw}^{\min}$ and $\Delta P_{iw}^{\max}$ are the lower and upper regulation bounds of the *w*th inverter in the *i*th sub-area, respectively; $P_{iw}^{\min}$ is the minimum operation power of the inverter; P_i^{si} is the power operation point of the specimen inverter at the *i*th sub-area; ΔP^{in} denotes the total regulation power input of the PV power plant; and P^{in} is the AGC signal of the PV power plant.

C. Optimization Model

In this work, the hierarchical CPC attempts to improve the responding performance of the whole PV power plant in response to the AGC signals from ISO, while the reactive power reserve is also considered. The responding performance can be quantitatively described with the power deviation between the AGC signal and the total regulation power output. Hence, the optimization model of the upper-layer CPC can be written as

$$\min f = \sum_{i=1}^{n} f_i\left(\Delta P_i^{\mathrm{in}}(k)\right) \quad (8)$$

$$\begin{cases} f_i\left(\Delta P_i^{\mathrm{in}}(k)\right) = \theta \cdot \Delta P_i^{\mathrm{D}}(k) + (1-\theta) \cdot \left(Q_i^{\max} - Q_i^{\mathrm{r}}(k)\right) \\ \Delta P_i^{\mathrm{D}}(k) = \sum_{h=k}^{k+\tau} \left| \Delta P_i^{\mathrm{in}}(k) - \sum_{w=1}^{m_i} \Delta P_{iw}^{\mathrm{out}}(h) \right| \\ Q_i^{\mathrm{r}}(k) = \sum_{w=1}^{m_i} Q_{iw}^{\mathrm{r}}(k)\,; \;\; Q_i^{\max} = \sum_{w=1}^{m_i} Q_{iw}^{\max} \end{cases} \tag{9}$$

$$Q_{iw}^{\mathrm{r}}(k) = \begin{cases} P_{iw}^{\mathrm{in}}(k) \cdot \tan\varphi\,, & \text{if } P_{iw}^{\mathrm{in}}(k) < S_{iw} \cdot \cos\varphi \\ \sqrt{(S_{iw})^2 - \left(P_{iw}^{\mathrm{in}}(k)\right)^2}\,, & \text{else} \end{cases} \tag{10}$$

$$Q_{iw}^{\max} = S_{iw} \cdot \sin\varphi \tag{11}$$

$$s.t. \begin{cases} \Delta P^{\mathrm{in}}(k) = \sum_{i=1}^{n} \Delta P_i^{\mathrm{in}}(k) \\ \Delta P_i^{\min}(k) \le \Delta P_i^{\mathrm{in}}(k) \le \Delta P_i^{\max}(k), i = 1,2,\dots,n \end{cases} \tag{12}$$

where f is the overall objective function of the upper-layer CPC; f_i is the objective function of the ith sub-area; ΔP_i^{in} is the regulation power input of the ith sub-area, i.e., the optimization variable of the upper-layer CPC; θ is the objective weight, in which a larger objective weight indicates a larger preference on the minimization of power deviation; ΔP_i^{D} is the power deviation of the ith sub-area; Q_i^{r} and $Q_i^{\max}$ are the current and the maximum reactive power reserves of the ith sub-area, respectively; Q_{iw}^{r} and $Q_{iw}^{\max}$ are the current and the maximum reactive power reserves of the wth inverter in the ith sub-area, respectively; m_i is the number of inverters in the ith sub-area; φ is the limited power factor (PF) angle [27], which is set to be with $\cos\varphi = 0.9$ in this work; S_{iw} is the rated capacity of the wth inverter in the ith sub-area; τ represents the maximum response time of all the inverters; $\Delta P_i^{\min}$ and $\Delta P_i^{\max}$ are the lower and upper regulation bounds of the ith sub-area, respectively, which are equal to the sum of that of the corresponding inverters.

Note that the reactive power reserves in Eqs. (10) and (11) are determined by the regulation power input and the PF constraint. As illustrated in Fig. 3, the feasible operating region of an inverter is significantly reduced with the PF constraint, while the reactive power reserve is also decreased.

Similarly, the optimization model of the lower-layer CPC in the ith sub-area can be written as

$$\min f_i = \sum_{w=1}^{m_i-1} f_{iw}\left(\Delta P_{iw}^{\mathrm{in}}(k)\right) \tag{13}$$

$$\begin{cases} f_{iw}\left(\Delta P_{iw}^{\mathrm{in}}(k)\right) = \theta \cdot \Delta P_{iw}^{\mathrm{D}}(k) + (1-\theta) \cdot \left(Q_{iw}^{\max} - Q_{iw}^{\mathrm{r}}(k)\right) \\ \Delta P_i^{\mathrm{D}}(k) = \sum_{h=k}^{k+\tau} \left| \Delta P_{iw}^{\mathrm{in}}(k) - \Delta P_{iw}^{\mathrm{out}}(h) \right| \end{cases} \tag{14}$$

$$s.t. \begin{cases} \Delta P_i^{\mathrm{in}}(k) = \sum_{w=1}^{m_i-1} \Delta P_{iw}^{\mathrm{in}}(k) \\ \text{Eqs. (4), (10), and (11)} \end{cases} \tag{15}$$

where f_{iw} is the objective function of the wth inverter in the ith sub-area and $\Delta P_{iw}^{\mathrm{in}}$ is also the optimization variable of the lower-layer CPC, excluding the specimen inverter.

III. FDAA FOR CPC

A. Graph Theory

The interactive network among different agents can be described as a graph $G = (V, E, A)$ with multiple nodes $V = \{v_1, v_2, \dots, v_n\}$ and edges $E \subseteq V \times V$, where v_i denotes the ith node (i.e., the ith agent); and $A = [a_{ij}] \in R^{n \times n}$ denotes a weighted adjacency matrix [28]. In this work, the constant a_{ij} is set to be 1 if there is an edge between v_i and v_j, otherwise $a_{ij} = 0$. Therefore, the set Ω_i of interactive agents for the ith agent can be written as follows:

$$\Omega_i = \left\{ v_j \in V \middle| a_{ij} = 1, j \ne i \right\} \tag{16}$$

B. Operators for Distributed Optimization of CPC

Like the original ADAA, each agent of FDAA will implement four operators, including bids evaluation, consensus procedure, auction resolution and swap operations, and swap size update [21]. Here, we mainly introduce these four operators for the upper-layer CPC, while the lower-layer CPC can be solved following the same operators.

a) Bids evaluation

In FDAA, each agent will play the part of a buyer or a seller to exchange power with its interactive agents. This power bid will result in an objective variation for the ith agent, as follows:

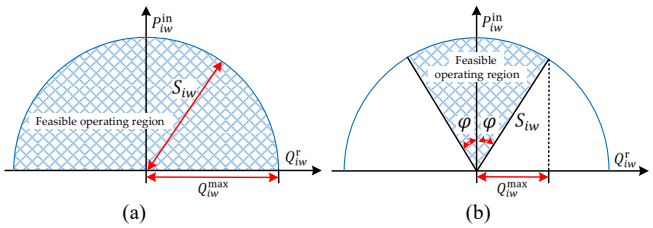

Fig. 3. Feasible operating region of an inverter considering the capacity constraint. (a) Without PF constraint and (b) With PF constraint.

$$\begin{cases} \pi_i = f_i\left(\Delta P_i^{\text{in}} + \Delta p_i\right) - f_i\left(\Delta P_i^{\text{in}}\right), \text{ if buy} \\ \mu_i = f_i\left(\Delta P_i^{\text{in}}\right) - f_i\left(\Delta P_i^{\text{in}} - \Delta p_i\right), \text{ if sell} \end{cases} \tag{17}$$

where π_i is the objective increment of the *i*th agent if its regulation power input increases Δp_i based on the current value ΔP_i^{in}; μ_i is the objective decrement of the *i*th agent; and Δp_i denotes the current swap size of the *i*th agent, with $\Delta p_i > 0$.

With the regulation power increment or decrement based on the current solution, the objective variation can be directly calculated based on Eqs. (9)-(11) and the optimization results from the lower-layer CPC.

b) Consensus procedure

This procedure is designed to satisfy the power balance constraint in Eq. (12), where each agent should reach a consensus on the power bidding with its interactive agent. If an agent increases Δp on the regulation power input, one of interactive agents should also decrease Δp on its regulation power input. Hence, the total objective decrement δ_{ij} caused by the power bid between the *i*th and the *j*th agents can be described as follows:

$$\delta_{ij} = \mu_j - \pi_i \tag{18}$$

Since each agent can exchange power with only one of other agents, it should select the best partner from the interactive agents. For a minimization, the interactive agent which can lead to the maximum objective decrement will be chosen as the best partner, as follows:

$$\delta_i^{\max} = \max_{j \in \Omega_i} \delta_{ij} \tag{19}$$

$$b_i = \operatorname*{argmax}_{j \in \Omega_i} \delta_{ij} \tag{20}$$

where $\delta_i^{\max}$ denotes the maximum objective decrement when the *i*th agent increases Δp_i on the regulation power input, while its interactive agents decrease their inputs by Δp_i; and b_i denotes the best partner of the *i*th agent.

c) Auction resolution and swap operations

If an agent can bring a positive and larger objective decrement than that of its interactive agents, the auction resolution will be reached between it and its best partner. For the *i*th agent, these conditions can be written as follows:

$$\begin{cases} \delta_i^{\max} > 0 \\ \delta_i^{\max} > \max\limits_{j \in \Omega_i} \delta_j^{\max} \end{cases} \tag{21}$$

If the conditions in Eq. (21) can be satisfied, a greedy search for a better solution can be achieved. This solution for the *i*th agent and its best partner can be updated as follows:

$$\begin{cases} \Delta P_i^{\text{in}}(l+1) = \Delta P_i^{\text{in}}(l) + \Delta p_i(l) \\ \Delta P_{b_i}^{\text{in}}(l+1) = \Delta P_{b_i}^{\text{in}}(l) + \Delta p_i(l) \end{cases} \tag{22}$$

where l denotes the iteration number in FDAA.

d) Swap size update

To accelerate the convergence rate, the swap size of each agent will be continuously adjusted to adapt the dynamic optimization results. For the *i*th agent, it can be updated as

$$\Delta p_i(l+1) = \begin{cases} \gamma \cdot \Delta p_i(l), & \text{if } \delta_i^{\max} > 0 \\ \Delta p_i(l)/\gamma, & \text{else} \end{cases} \tag{23}$$

where γ denotes the gain factor, with $\gamma > 1$.

To satisfy power balance constraint in Eq. (12), the sum of the initial regulation power inputs of all the sub-areas should be equal to the total regulation power input. Moreover, the regulation power input of each sub-area should be limited within the lower and upper bounds for the regulation power capacity constraints in Eq. (12). Here, they can be written as

$$\Delta P_i^{\text{in}}(l=1) = \Delta P^{\text{in}} \cdot \frac{\Delta P_i^{\max} - \Delta P_i^{\min}}{\sum_{j=1}^{n}\left(\Delta P_j^{\max} - \Delta P_j^{\min}\right)} \tag{24}$$

$$\Delta P_i^{\text{in}}(l) = \begin{cases} \Delta P_i^{\min}, & \text{if } \Delta P_i^{\text{in}}(l) < \Delta P_i^{\min} \\ \Delta P_i^{\max}, & \text{if } \Delta P_i^{\text{in}}(l) > \Delta P_i^{\max} \end{cases} \tag{25}$$

C. Random Forest based Dynamic Surrogate Model

As given in Eq. (17), each agent should implement two bid evaluations to acquire the objective increment and decrement at each iteration. Note that one bid evaluation of each agent in the upper-layer CPC can be determined only based on the optimization results of the lower-layer CPC. As a result, it will cause a high computation cost and a large number of communications in the lower-layer CPC when the upper-layer CPC is accomplished. To handle this problem, a random forest [23] is used to construct a dynamic surrogate model of the lower-layer CPC. Hence, FDAA can implement a fast solution evaluation for the upper-layer CPC based on this dynamic surrogate model instead of the optimization results of the lower-layer CPC.

The random forest [29] is essentially an ensemble learning method, which is formed by multiple classification and regression trees (CARTs), as shown in Fig. 4. It is suitable to construct the dynamic surrogate model of the lower-layer CPC attributed to its

fast training rate and high generalization ability. For the *i*th sub-area, the training process of random forest mainly includes four steps [30], as follows:

●***Step 1***: generate the training data $\Delta P_i^{\text{in}} \rightarrow f_i$ via an uniform selection of power command from the lower bound to the upper bound, in which the inputs of training data can be determined as:

$$x_h = \Delta P_i^{\min} + \frac{h-1}{H-1} \cdot \left(\Delta P_i^{\max} - \Delta P_i^{\min}\right) \tag{26}$$

where x_h is the input of the *h*th training sample and *H* is the number of training samples.

Here, the outputs of training data is the optimization results of Eqs. (13)-(15) by the same operations of ADAA with Eqs. (17)-(25).

●***Step 2***: randomly generate the sample sub-set for each CART based on the original training data.

●***Step 3***: implement a training for each CART via the recursive constructions of binary decision tree, in which the splitting variable *e* and the splitting point *s* can be recursively determined based on the following minimization:

$$\min_{e,s}\left[\min_{c_1}\sum_{x_h \in R_1(e,s)}(y_h - c_1)^2 + \min_{c_2}\sum_{x_h \in R_2(e,s)}(y_h - c_2)^2\right] \tag{27}$$

where $R_1(e,s)$ and $R_2(e,s)$ are the subregions for $x_h < s$ and $x_h \geq s$, respectively; y_h is the output corresponding to x_h; c_1 and c_2 are the output mean values in $R_1(e,s)$ and $R_2(e,s)$, respectively.

●***Step 4***: construct all the trained CARTs into a forest, in which the output of random forest is equal to the average of all the CARTs, as

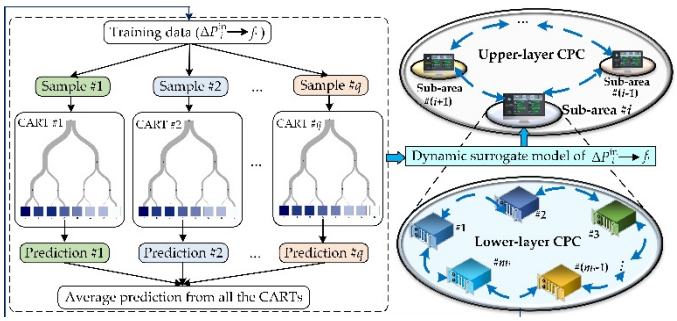

Fig. 4. Random forest based dynamic surrogate model for CPC.

TABLE I

THE DETAILED EXECUTION PROCEDURE OF FDAA FOR HIERARCHICAL CPC

Initialize the interactive networks and parameters of FDAA;
FOR1 *i*:=1 to *n*
  Acquire the real-time power outputs of all the inverters;
  Evaluate the regulation capabilities of all the inverters by Eqs. (4)-(7);
  Determine the inputs of the training data of the *i*th sub-area by Eq. (26);
  Acquire the outputs of the training data by step 22 to step 32;
  Generate the dynamic surrogate model of the *i*th sub-area by random forest;
END FOR1
Input the real-time total regulation power input ΔP^{in} of the PV power plant;
Set *l*:=1;
Initialize the solutions of the upper-layer CPC by Eq. (24);
WHILE1 $l \leq l_{\text{up}}^{\max}$
  FOR2 *i*:=1 to *n*
    Evaluate the objective variations by Eqs. (17) and (28);
    Find the best partner of the *i*th sub-area by Eqs. (18)-(20);
    Update the solution of the *i*th sub-area by Eqs. (21)-(22) and (25);
    Adjust the swap size of the *i*th sub-area by Eq. (23);
  END FOR2
  Set *l*:=*l*+1;
END WHILE1
Output the optimal regulation power inputs of all the sub-areas;
FOR3 *i*:=1 to *n*
  Set *l*:=1;
  Initialize the solutions of the lower-layer CPC in the *i*th sub-area by Eq. (24);
  WHILE2 $l \leq l_{\text{low}}^{\max}$
    FOR4 *j*:=1 to m_i-1
      Evaluate the objective variations by Eqs. (17);
      Find the best partner of the *j*th inverter by Eqs. (18)-(20);
      Update the solution of the *j*th inverter by Eqs. (21)-(22) and (25);
      Adjust the swap size of the *j*th inverter by Eq. (23);
    END FOR4
    Set *l*:=*l*+1;
  END WHILE2
END FOR3
Output the optimal regulation power inputs of all the inverters;

36: Re-generate the dynamic surrogate models by step 2 to step 8;
37: Re-execute the operations from step 9 to step 35 for the next AGC signal.

$$y = \frac{1}{q}\sum_{u=1}^{q}\sum_{m=1}^{M_u} c_m^u I(x \in R_m^u) \tag{28}$$

where q is the number of CARTs; M_u is the number of subregions of the uth CART; R_m^u denotes the mth subregion of the uth CART; c_m^u is the output mean value in R_m^u; and I is the input value in R_m^u.

D. Execution Procedure

Taken together, the execution procedure of FDAA for CPC can be given in Table I, where $l_{\text{up}}^{\max}$ and $l_{\text{low}}^{\max}$ are the maximum iteration numbers for the upper-layer CPC and the lower-layer CPC, respectively. Note that the random forest based dynamic surrogate model is mainly used to decouple the upper-layer CPC and lower-layer CPC instead of the problem solving for Eqs. (13)-(15). As shown in Table I, the lower-layer CPC will be solved by the original ADAA from step 23 to step 33 after the upper-layer CPC is solved by FDAA step 10 to step 20. In the random forest, a larger number of CARTs and a larger H will lead to higher regression accuracy and generalization ability, but it also consumes more computation time. Hence, both of them can be set with a proper balance between regression accuracy and computation time through trial-and-error.

If the upper-layer CPC is solved by the original ADAA without the random forest model, the number of total iterations for these two-layer optimizations is equal to $\left(l_{\text{up}}^{\max} + 2 \cdot l_{\text{up}}^{\max} \cdot l_{\text{low}}^{\max} + l_{\text{low}}^{\max}\right)$. In contrast, the number of total iterations by FDAA is equal to $\left(l_{\text{up}}^{\max} + l_{\text{low}}^{\max}\right)$, which is much smaller than that without the random forest based dynamic surrogate model.

E. Discussion of Optimality

The global convergence of ADAA has been proven in [21] based on the assumption that the maximum iteration number is infinite. It is impractical for the hierarchical CPC with a short time cycle. Hence, both of ADAA and FDAA can only acquire a high-quality optimum to approximate the global optimum as close as possible within a limited number of iterations.

IV. Case Studies

The testing system is a PV power plant with 10 sub-areas and 100 inverters, in which each sub-area consists of 10 PV arrays and 10 inverters with a specimen inverter. The rated capacity of each inverter is 0.5 MW, the minimum power output of each inverter is set to be 40% of the current power output of the corresponding specimen inverter. The initial power output of each inverter is set to be 0.3 MW. Moreover, the delay and regulation time constants of each inverter can be determined as their average values of the actual operating data, which can be updated weekly or monthly. In this work, these time constants are artificially designed to simulate the actual operating data, as given in Fig. 5. The objective weight θ is set to be 0.5 by considering the same preference on the power deviation and the reactive power reserve.

In [21], an interactive network with more edges will accelerate the convergence of ADAA, while the interactions and computations will directly increase. To reduce the interactions and computations, the interactive network among all the sub-areas is designed as a ring network (See Fig. 6), as well as for the inverters in each sub-area. Besides, the main parameters of FDAA are given in Table II, where number of CARTs in the random forest is set to be 40 since the regression accuracy is difficult to dramatically improve when it is larger than 40. To evaluate the performance of FDAA, the frequently-used engineering method [10] is introduced for comparison, which allocates the total power regulation input to all the inverters in proportional to their regulation capacities. This method is implemented under the direct and hierarchical control frameworks [12], respectively. To distinguish these two frameworks, the delay time constant of each inverter under the direct control framework is set to be two times of that in Fig. 4(a) under the hierarchical control framework.

A. Study with a Constant Irradiation

Here, the irradiations of all the sub-areas are set to the standard value, i.e., 1000 W/m^2.

a) Study of dynamic surrogate model

To construct the dynamic surrogate model for each sub-area, it should firstly provide the training data via the original ADAA for the pre-designed optimization tasks. Fig. 7 shows the convergence process of the lower-layer CPC of the sub-area #1 at the 18$^{\text{th}}$ optimization task ($\Delta P_1^{\text{in}} = 1.395$ MW). It clearly shows that all the inverters can rapidly converge to the optimal solution within 30 iterations by gradually adjusting the step size.

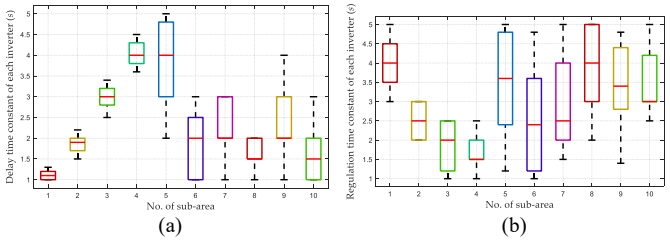

(a) (b)

Fig. 5. The parameter distribution of each inverter in each sub-area. (a) Delay time constant and (b) Regulation time constant.

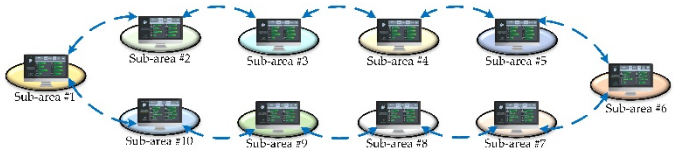

Fig. 6. Interactive network among all the sub-areas.

TABLE II
MAIN PARAMETERS OF FDAA

$l_{\text{up}}^{\max}$	$l_{\text{low}}^{\max}$	$\Delta p_{\text{up}}(l=0)$	$\Delta p_{\text{low}}(l=0)$	γ	H	q
50	50	0.1	0.01	2	21	40

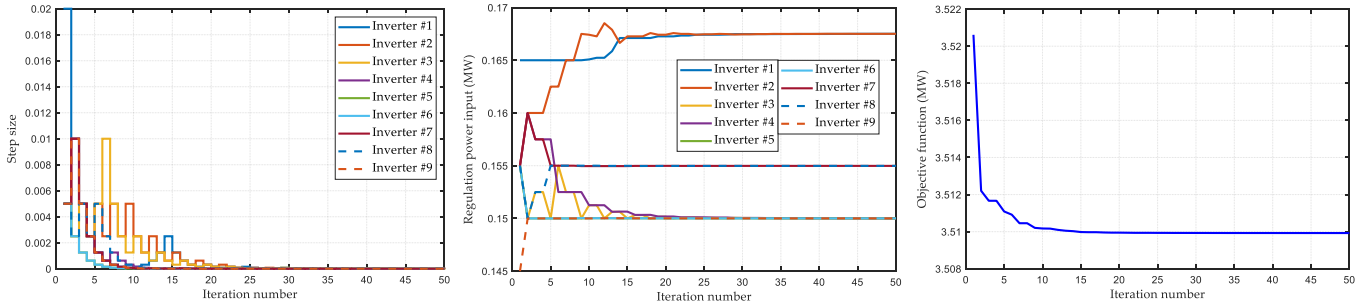

(a) (b) (c)

Fig. 7. Convergence process of FDDA for lower-layer CPC of sub-area #1. (a) Step size, (b) Regulation power input, and (c) Objective function.

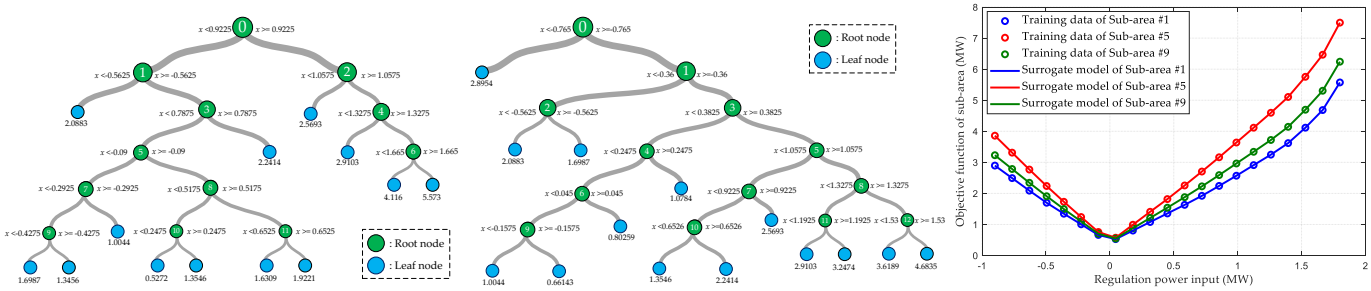

(a) (b) (c)

Fig. 8. Training results of random forest for some sub-areas. (a) CART #3 of random forest for sub-area #1, (b) CART #6 of random forest for sub-area #1, and (c) Regression curves.

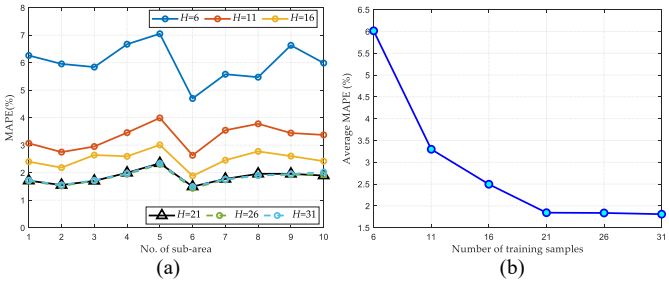

(a) (b)

Fig. 9. MAPE of random forest with different numbers of training samples. (a) MAPE of each sub-area and (b) Average MAPE.

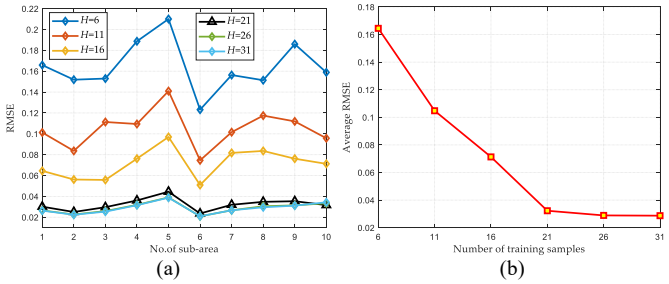

(a) (b)

Fig. 10. RMSE of random forest with different numbers of training samples. (a) RMSE of each sub-area and (b) Average RMSE.

Fig. 8 gives the training results of random forest for the dynamic surrogate model. It can be found from Fig. 8(a)-(b) that the generated CART #1 and CART #3 are different due to their different training samples, thus the random forest with multiple CARTs can dramatically enhance the ability to avoid over-fitting compared with a single CART. Consequently, the random forest can provide a reliable dynamic surrogate model for each sub-area, as the surrogate models for sub-areas (#1, #5, #9) shown in Fig. 8(c).

To evaluate the performance of random forest with different number of training samples, the means absolute percentage error

(MAPE) and the root mean squared error (RMSE) [31] are employed to evaluate the regression accuracy. As shown in Figs. 9 and 10, both of MAPE and RMSE for each sub-area decrease as the number of training samples increases. However, it only acquires a negligible decrement for these two indices when the number of training samples is larger than 21. Therefore, the number of training samples is set to be 21 in other case studies.

b) Study of a step AGC signal

Here, a step AGC signal ($P^{\text{in}} = 40$ MW) at the 5$^{\text{th}}$ second is introduced to test the responding performance with different methods, as illustrated in Fig. 11. Although all the sub-areas have the same reserve capacities, but they are assigned by different AGC signals (See Fig. 11(a)) by FDAA due to their difference on the delay and regulation time constants. Compared with the engineering method with direct control (EMDC) and hierarchical control (EMHC), FDAA can acquire a better power output curve which can approximate the AGC signal more close, as shown in Fig. 11(b). Besides, the reactive power reserve shows no apparent difference among three method, but that of each method is obviously higher than that without the AGC signal, as shown in Fig. 11(c).

Fig. 12 gives the convergence process of FDAA with ($P^{\text{in}} = 40$ MW). It shows that the surrogate model based FDAA can acquire the step size curve, overall objective function curve, and optimal solution that are close to that of the original ADAA without surrogate model. It also reveals that random forest can achieve a high regression performance, thus a reliable surrogate model can effectively accelerate the optimization of FDAA. On the other hand, it can be found that the convergence speeds of FDAA and ADAA without surrogate model are almost the same. However, FDAA can rapidly implement a bid evaluation for the upper-layer CPC based on the surrogate model at each iteration. In contrast, ADAA can implement the same operator only based on the optimization results of the lower-layer CPC, which consumes additional 50 iterations for each sub-area in the lower-layer CPC. Hence, the convergence speed of FDAA is much faster than that of ADAA without the surrogate model.

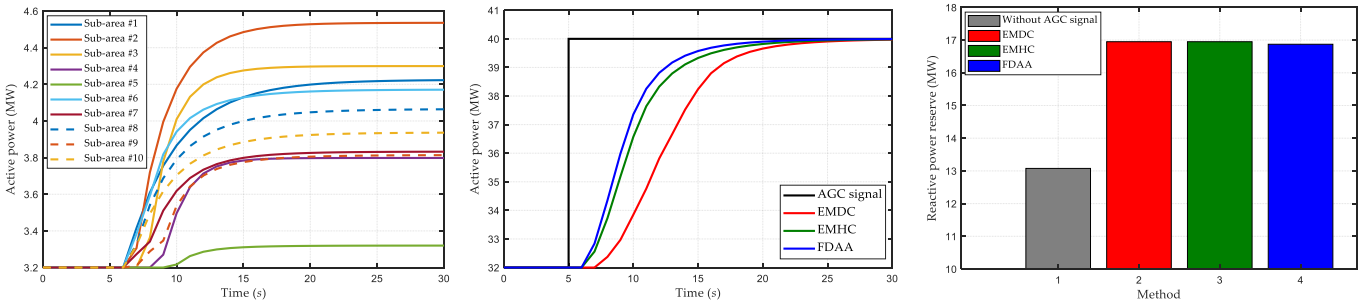

(a) (b) (c)

Fig. 11. Responding performance with a step AGC signal under a constant irradiation. (a) AGC signal of each sub-area by FDAA, (b) Overall responding power by different algorithms, and (c) Reactive power reserve by different algorithms.

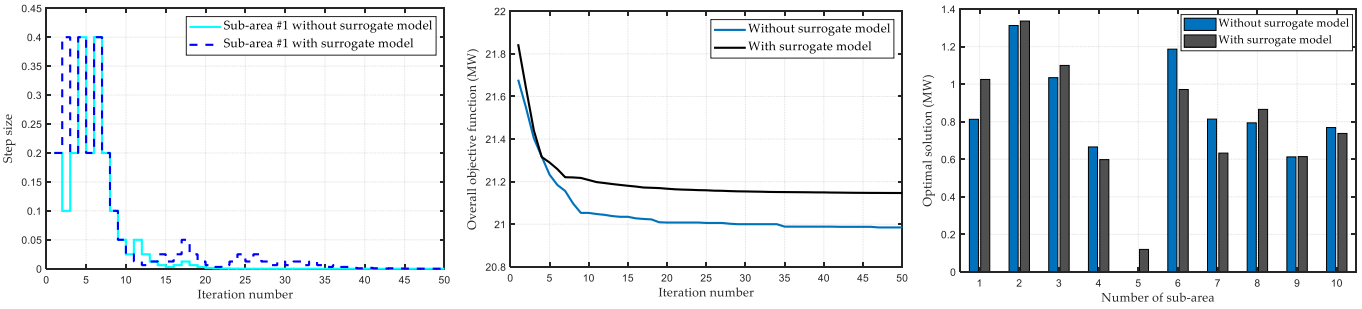

(a) (b) (c)

Fig. 12. Convergence process of FDDA for upper-layer CPC with a step AGC signal. (a) Step size, (b) Objective function, and (c) Optimal solution.

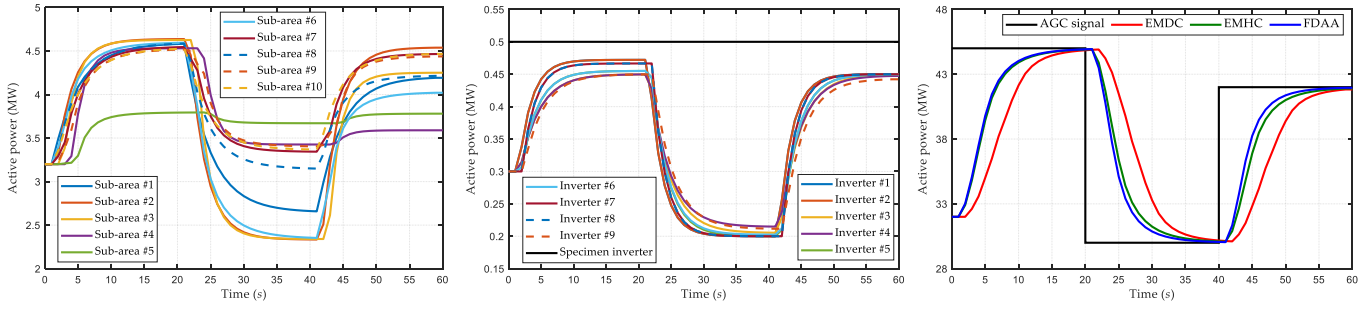

(a) (b) (c)

Fig. 13. Responding performance with continuous step AGC signals under a constant irradiation. (a) AGC signal of each sub-area by FDAA, (b) AGC signal of each inverter in sub-area #2 by FDAA, and (c) Overall responding power by different algorithms.

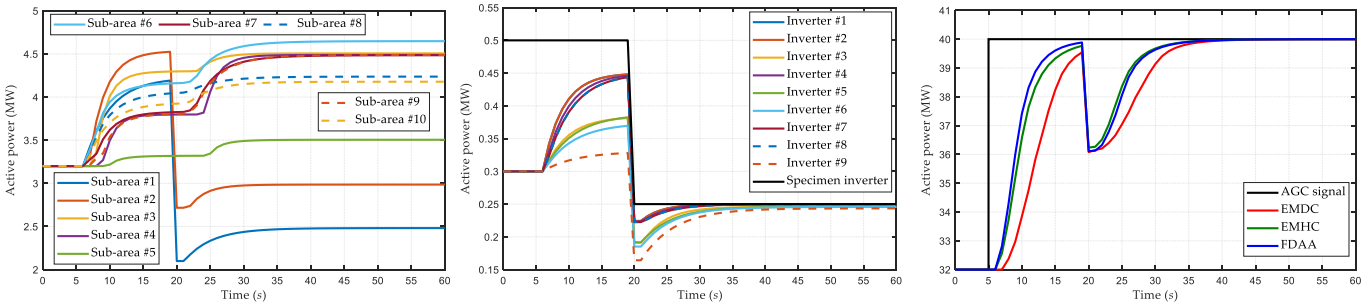

(a) (b) (c)

Fig. 14. Responding performance with a step AGC signal under varying irradiations. (a) AGC signal of each sub-area by FDAA, (b) AGC signal of each inverter in sub-area #2 by FDAA, and (c) Overall responding power by different algorithms.

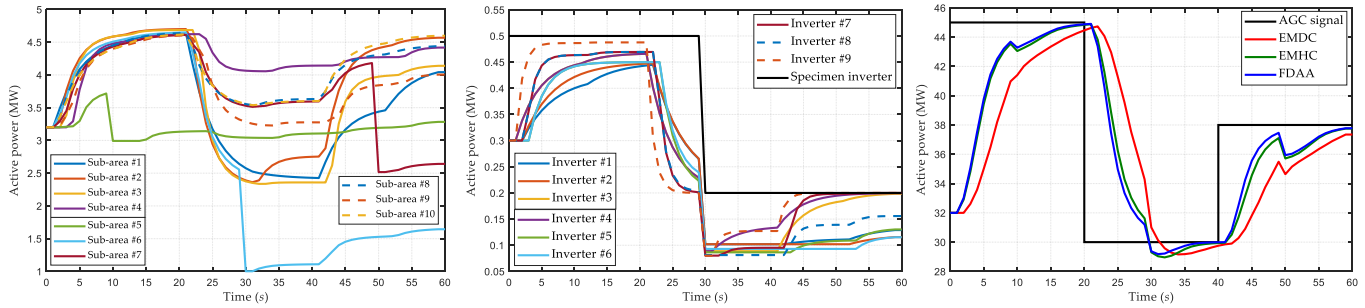

(a) (b) (c)

Fig. 15. Responding performance with continuous AGC signals under varying irradiations. (a) AGC signal of each sub-area by FDAA, (b) AGC signal of each inverter in sub-area #6 by FDAA, and (c) Overall responding power by different algorithms.

c) Study of continuous step AGC signals

Here, the continuous step AGC signals is designed to test the responding performance with different methods, as given in Fig. 13. Fig. 13(a) shows that the sub-area #2 is assigned with a large part of the total AGC signal compared with other sub-areas due to the high regulation performance of its inverters. Similarly, the overall power output curve obtained by FDAA is closer to the continuous AGC signals against to EMDC and EMHC. It also verifies the effectiveness of distributed optimization for CPC by FDAA.

TABLE III
STATISTICAL RESULTS OBTAINED BY DIFFERENT METHODS

Irradiation	AGC signal	Power deviation (MW)			Reactive power reserve (Mvar)		
		EMDC	EMHC	FDAA	EMDC	EMHC	FDAA
Constant	A step	66.44	47.04	**41.53**	16.63	16.63	16.56
	Continuous	328.50	232.93	**213.42**	16.47	16.47	16.06
Varying	A step	96.92	68.41	**64.98**	16.95	16.95	16.63
	Continuous	311.79	224.05	**205.74**	15.82	15.82	15.52

B. Study with Varying Irradiations

a) Study of a step AGC signal

Here, the initial irradiations of all the sub-areas are set to be 1000 W/m^2, in which the irradiations of the sub-areas #1 and #2 are respectively changed to 500 W/m^2 and 600 W/m^2 at the 20th second. Fig. 14 shows the responding performance with a step AGC signal under these varying irradiations. It illustrates that FDAA can re-optimize the regulation power of all the sub-areas or inverters to match the varying irradiations of sub-area #1 and #2. Besides, it also can be found that the overall power output obtained by FDAA can respond the AGC signal more closely than other two methods.

b) Study of continuous step AGC signals

Here, the initial irradiations of all the sub-areas are set to be 1000 W/m^2, in which the irradiations of the sub-areas #5 to #7 are changed to 800 W/m^2, 400 W/m^2, and 600 W/m^2 at the 10th, 30th, and 50th seconds, respectively. Fig. 15 shows the responding performance with continuous AGC signals under these varying irradiations. Similarly, the overall power output can easily drop when the irradiations of the sub-areas #5 to #7 suddenly reduce. However, the power output obtained by FDAA can rapidly recover to trace the continuous step AGC signals via re-assigning the AGC signals for all the sub-areas and the inverters.

C. Discussions of Implementation Time

Since the maximum iteration number is set to be 50 at each layer, the numbers of total iterations by ADAA and FDAA are equal to 5100 and 100 for the hierarchical CPC, respectively. Particularly, the computation speed of FDAA is 51 times of that by ADAA without the random forest based surrogate model. Based on the testing system, both of ADAA and FDAA will 20 communications

at each iteration under the ring network for the upper-layer CPC, and 18 communications for each sub-area in the lower-layer CPC. Hence, the total number of communications by FDAA is only 1.10% of that by ADAA. This also verifies that the random forest based surrogate model not only can accelerate the computation speed of FDAA, but also can dramatically reduce the total number of communications.

According to the coverage range of different wireless technologies [32], the GSM wireless technology is employed for agents' communications of the upper-layer CPC, and the Zigbee [33] is adopted for the low-layer CPC with a shorter communication range. Based on these two wireless technologies, the total time of the information calculation and transmission will be shorter than 1 *ms* for each iteration of FDAA based on the ordinary calculation rate and data communication rate [32], as well as for the original ADAA. Since the two-layer optimizations of CPC can be decoupled with the random forest based dynamic surrogate model, the total implementation time of FDAA for the whole control process is smaller than 0.1 *s* ((50+50)×0.001) with the 50 iterations at each layer. Hence, FDAA is fast enough for online system control as its implementation time is shorter than the time cycle of AGC (1 to 16 *s*) [8].

D.Discussions of Statistical Results

Table III gives the statistical results obtained by different methods under different irradiations and AGC signals, where the power deviation denotes a sum value and the reactive power reserve denotes an average value. Collectively, FDAA can acquire a smaller power deviation than other two methods without optimization. Particularly, the power deviation obtained by FDAA is about 62.51% of that by EMDC with a step AGC signal under a constant irradiation. Since EMDC and EMHC allocate the total power regulation input in proportional to the regulation capacities of all the inverters, their obtained reactive power reserves are the same, which are slightly larger than that obtained by FDAA.

V.CONCLUSION

In this work, a novel distributed optimization algorithm is proposed for allocating the total AGC signal to all the inverters in a large-scale PV power plant, in which the main contributions can be summarized as follows:

1) The constructed CPC provides an effective way to a large-scale PV power plant for optimally responding the AGC signals via coordinating multiple inverters.

2) Compared with the frequently-used power allocation methods, the proposed FDAA can obtain a higher quality solution in a distributed way. As a result, the dynamic responding performance of the PV power plant can be dramatically improved for AGC.

3) The random forest based dynamic surrogate model can directly reduce the interaction between the low-layer CPC to the upper-layer CPC. Consequently, FDAA can be available to rapidly obtain an optimal allocation scheme for multiple inverters with lower computation and communication costs.

In this work, both the reactive power dispatch and the power loss in a PV power plant are not considered. From the viewpoint for real implementation, FDAA does not consider the influence by a practical communication network with transmission delay and noise. Besides, the quality of the obtained optimum by FDAA is impacted by the regression error of random forest. Consequently, our future works will focus on a comprehensive CPC by considering these factors, while an improved distributed optimization algorithm will be studied for real implementation.

REFERENCES

[1] X. Zhang, Z. Xu, and T. Yu *et al.* "Optimal mileage based AGC dispatch of a GenCo," *IEEE Trans. Power Syst.*, vol. 35, no. 4, pp. 2516-2526, Jul. 2020.

[2] B. K. Sahu, "A study on global solar PV energy developments and policies with special focus on the top ten solar PV power producing countries," *Renew. Sustain. Energy Rev.*, vol. 43, pp. 621-634, Mar. 2015.

[3] P. C. Sekhar and S. Mishra, "Storage free smart energy management for frequency control in a diesel-PV-fuel-cell-based hybrid AC microgrid," *IEEE Trans. Neural Netw. Learn. Syst.*, vol. 27, no. 8, pp. 1657-1671, Aug. 2016.

[4] Y. Arya, "AGC of PV-thermal and hydro-thermal power systems using CES and a new multi-stage FPIDF-(1+PI) controller," *Renew. Energy*, vol. 134, pp. 796-806, Apr. 2019.

[5] J. Hu, J. Zhu, and D. G. Dorrell, "Model predictive control of grid-connected inverters for PV systems with flexible power regulation and switching frequency reduction," *IEEE Trans. Ind. Appl.*, vol. 51, no. 1, pp. 587-594, Jan.-Feb. 2015.

[6] C. Zhong, Y. Zhou, and G. Yan, "A novel frequency regulation strategy for a PV system based on the curtailment power-current curve tracking algorithm," *IEEE Access.*, vol. 8, pp. 77701-77715, 2020.

[7] Q. Peng, Y. Yang, and T. Liu *et al.* "Coordination of virtual inertia control and frequency damping in PV systems for optimal frequency support," *CPSS Trans. Power Electron. Appl.*, vol. 5, no. 4, pp. 305-316, Dec. 2020.

[8] X. S. Zhang, T. Yu, and Z. N. Pan *et al.* "Lifelong learning for complementary generation control of interconnected power grids with high-penetration renewables and EVs," *IEEE Trans. Power Syst.*, vol. 33, no. 4, pp. 4097-4110, Jul. 2018.

[9] J. Li, T. Yu, and X. Zhang *et al.* "Efficient experience replay based deep deterministic policy gradient for AGC dispatch in integrated energy system," *Appl. Energy*, vol. 285, 116386, Jan. 2021.

[10] M. Datta, and T. Senjyu, "Fuzzy control of distributed PV inverters/energy storage systems/electric vehicles for frequency regulation in a large power system," *IEEE Trans. Smart Grid*, vol. 4, no. 1, pp. 479-488, Mar. 2013.

[11] P. Moutis, A. Vassilakis, and A. Sampani *et al*. "DC switch driven active power output control of photovoltaic inverters for the provision of frequency regulation," *IEEE Trans. Sustain. Energy*, vol. 60, no. 4, pp. 1485-1493, Oct. 2015.

[12] S. Wang, S. Duan, and W. Hou *et al*. "Three-level AGC for large-scale PV power plant with string inverters," in *Proc. IEEE Int. Conf. Power Syst. Technol.*, Wollongong, NSW, Australia, 2016, pp. 1-5

[13] R. Turner, S. Walton and R. Duke, "Stability and bandwidth implications of digitally controlled grid-connected parallel inverters," *IEEE Trans. Ind. Electron.*, vol. 57, no. 11, pp. 3685-3694, Nov. 2010.

[14] J. Giri, M. Parashar, and J. Trehern *et al*. "The situation room: Control center analytics for enhanced situational awareness," *IEEE Power Energy Mag.*, vol. 10, no. 5, pp. 24-39, Sep. 2012

[15] M. D. Ilić, L. Xie, and U. A. Khan *et al*. "Modeling of future cyber-physical energy systems for distributed sensing and control," *IEEE Trans. Syst., Man Cybern., A, Syst. Humans*, vol. 40, no. 4, pp. 825-838, Jul. 2010.

[16] Z. Zhang and M.-Y. Chow, "Convergence analysis of the incremental cost consensus algorithm under different communication network topologies in a smart grid," *IEEE Trans. Power Syst.*, vol. 27, no. 4, pp. 1761 – 1768, Nov. 2012.

[17] X. Zhang, H. Xu, and T. Yu *et al*. "Robust collaborative consensus algorithm for decentralized economic dispatch with a practical communication network," *Electric Power Syst. Res.*, vol. 140, pp. 597-610, Nov. 2016.

[18] G. Chen and Q. Yang, "An ADMM-based distributed algorithm for economic dispatch in islanded microgrids," *IEEE Trans. Ind. Informat.*, vol. 14, no. 9, pp. 3892-3903, Sep. 2018.

[19] A. Erdeljan, D. Capko, and S. Vukmirovic *et al*. "Distributed PSO algorithm for data model partitioning in power distribution system," *J. Appl. Res. Technol.*, vol. 12, vo. 5, pp. 947-957, Oct. 2014.

[20] G. Binetti, A. Davoudi, and D. Naso *et al.* "A distributed auction-based algorithm for nonconvex economic dispatch problem," *IEEE Trans. Power Syst.*, vol. 10, no. 2, pp. 1124-1132, May 2014.

[21] X. Zhang, T. Tan, and B. Zhou *et al.* "Adaptive distributed auction-based algorithm for optimal mileage based AGC dispatch with high participation of renewable energy," *Int. J. Electr. Power Energy Syst.*, vol. 124, 106371, Jan. 2021.

[22] Y. Jin, H. Wang, and T. Chugh *et al.* "Data-driven evolutionary optimization: An overview and case studies," *IEEE Trans. Evol. Comput.*, vol. 23, vo. 3, pp. 442-458, Jun. 2019.

[23] H. Wang and Y. Jin, "A random forest-assisted evolutionary algorithm for data-driven constrained multiobjective combinatorial optimization of trauma systems," *IEEE Trans. Cybern.*, vol. 50, vo. 2, pp. 536-549, Feb. 2020.

[24] B. Hafez, H. S. Krishnamoorthy, and P. Enjeti *et al.* "Medium voltage AC collection grid for large scale photovoltaic plants based on medium frequency transformers," in *Proc. IEEE Energy Convers. Congr. Expo. (ECCE)*, Sep. 2014, pp. 5304-5311.

[25] J. Wang, X. Mu, and Q. Li, "Study of passivity-based decoupling control of T-NPC PV grid-connected inverter," *IEEE Trans. Ind. Electron.*, vol. 64, no. 9, pp. 7542-7551, Sept. 2017.

[26] A. Sadeghi-Mobarakeh and H. Mohsenian-Rad, "Optimal bidding in performance-based regulation markets: An MPEC analysis with system dynamics," *IEEE Trans. Power Syst.*, vol. 32, no. 2, pp. 1282-1292, Mar. 2017.

[27] D. Yang, X. Wang, and F. Liu *et al.* "Adaptive reactive power control of PV power plants for improved power transfer capability under ultra-weak grid conditions," *IEEE Trans. Smart Grid*, vol. 10, vo. 2, pp. 1269-1279, Mar. 2019.

[28] C. D. Godsil and G. Royle, *Algebraic Graph Theory*. New York, NY, USA: Springer-Verlag, 2001.

[29] L. Breiman, "Random forests," *Mach. Learn.*, vol. 45, no. 1, pp. 5-32, 2001.

[30] Y. Zhao, X. Zhao, and L. Yan *et al.* "Reconstruction of the statistical characteristics of electric fields in enclosures with an aperture based on random forest regression," *IEEE Trans. Electromagn. Compat.*, vol. 62, vo. 4, pp. 1151-1159, Aug. 2020.

[31] Q. Zhang, L. T. Yang, and Z. Yan *et al.* "An efficient deep learning model to predict cloud workload for industry informatics," *IEEE Trans. Ind. Informat.*, vol. 14, no. 7, pp. 3170-3178, Jul. 2018.

[32] J. E. Shuda, A. J. Rix and M. J. Booysen, "Towards module-level performance and health monitoring of solar PV plants using LoRa wireless sensor networks," *2018 IEEE PES/IAS PowerAfrica*, 2018, pp. 172-177, doi: 10.1109/PowerAfrica.2018.8521179.

[33] M. E. Andreoni López, F. J. Galdeano Mantiñan and M. G. Molina, "Implementation of wireless remote monitoring and control of solar photovoltaic (PV) system," *2012 Sixth IEEE/PES Transmission and Distribution: Latin America Conference and Exposition (T&D-LA)*, 2012, pp. 1-6, doi: 10.1109/TDC-LA.2012.6319050.